Uniqueness of Elastoplastic Properties Measured by Instrumented Indentation

6

L. Liu, Xi Chen, N. Ogasawara, and N. Chiba

Contents

L. Liu (✉)
Department of Mechanical and Aerospace Engineering, Utah State University, Logan, UT, USA
e-mail: ling.liu@usu.edu

X. Chen (✉)
Department of Earth and Environmental Engineering, Columbia Nanomechanics Research
Center, Columbia University, New York, NY, USA
e-mail: xichen@columbia.edu

N. Ogasawara (✉)
Department of Mechanical Engineering, National Defense Academy of Japan, Yokosuka, Japan
e-mail: oga@nda.ac.jp

N. Chiba
National Defense Academy of Japan, Yokosuka, Japan
e-mail: chiba@nda.ac.jp

Abstract

Indentation is widely used to extract material elastoplastic properties from the measured load-displacement curves. One of the most well-established indentation technique utilizes dual (or plural) sharp indenters (which have different apex angles) to deduce key parameters such as the elastic modulus, yield stress, and work-hardening exponent for materials that obey the power-law constitutive relationship. Here we show the existence of "mystical materials," which have distinct elastoplastic properties, yet they yield almost identical indentation behaviors, even when the indenter angle is varied in a large range. These mystical materials are, therefore, indistinguishable by many existing indentation analyses unless extreme (and often impractical) indenter angles are used. Explicit procedures of deriving these mystical materials are established, and the general characteristics of the mystical materials are discussed. In many cases, for a given indenter angle range, a material would have infinite numbers of mystical siblings, and the existence maps of the mystical materials are also obtained. Furthermore, we propose two alternative techniques to effectively distinguish these mystical materials. In addition, a critical strain is identified as the upper bound of the detectable range of indentation, and moderate tailoring of the constitutive behavior beyond this range cannot be effectively detected by the reverse analysis of the load-displacement curve. The topics in this chapter address the important question of the uniqueness of indentation test, as well as providing useful guidelines to properly use the indentation technique to measure material elastoplastic properties.

Keywords

Indentation · Elastoplastic properties · Unique solution · Numerical study · Indistinguishable load-displacement curve · Reverse analysis · Detectable strain range · Critical strain · Loading curvature · Indenter angle

Introduction

Instrumented indentation is widely used to probe the constitutive relationships of engineering materials. Without losing generality, the uniaxial true stress-strain curve of a stress-free elastoplastic solid can be expressed in a power-law form, which is a

good approximation for most metals and alloys (Cheng and Cheng 2004).

$$\sigma = E\varepsilon \text{ for } \varepsilon \leq \frac{\sigma_y}{E} \text{ and } \sigma = \sigma_y \left(\frac{E}{\sigma_y}\right)^n \varepsilon^n = R\varepsilon^n, \tag{1}$$

where E is the Young's modulus, σ_y is the yield stress, and n is the work-hardening exponent. For most metals and alloys, n is between 0.0 and 0.5, E is between 10 and 600 GPa, σ_y is between 10 and 2000 MPa, and E/σ_y is between 100 and 5000 (Ashby 1999) – this is a technical range of the engineering materials suitable for the conventional indentation analysis where finite strains are involved.

Four independent parameters (E, ν, σ_y, n) are needed to completely characterize the elastoplastic properties of a power-law stress-free material. Probing these material parameters by indentation has become a focal point of interest in the indentation literature, and various techniques were proposed; see the review by Cheng and Cheng (2004). However, even for some of the existing techniques that are considered as "well-established," the fundamental question of whether the elastoplastic properties of a specimen can be uniquely determined is still open.

For any indentation technique, the existence of a unique solution requires that the indentation response must be unique for a given material, i.e., one-to-one correspondence between the shape factors of the measured indentation load-displacement curves and material elastoplastic properties. For example, when the apex angle of a sharp indenter is fixed, several research groups have shown that a set of special materials with distinct elastoplastic properties may yield almost the same indentation load-displacement curves (Cheng and Cheng 1999; Capehart and Cheng 2003; Tho et al. 2004; Alkorta et al. 2005). Therefore, the mechanical properties of these specimens cannot be uniquely determined by using one sharp indenter.

In this chapter based on Chen et al. (2007) and Liu et al. (2009), we carry out a systematic numerical study to correlate the indentation responses with a wide range of material properties and a variety of indenter geometries and present an explicit formulation to determine the special sets of materials with distinct elastoplastic properties yet exhibit indistinguishable indentation behaviors even when different indenters are employed. We call such sets of special materials as *mystical materials* – i.e., they are beyond the previous (and conventional) understanding of this topic. For many power-law materials, they have infinite mystical siblings that have indistinguishable loading and unloading behaviors during the indentation test, for a wide range of indenter geometries. Due to the lack of unique solutions, theoretically, these mystical materials are unable to be distinguished by many previously established techniques, including the dual (or plural) sharp indentation method and the conventional spherical indentation analysis with small penetration. The existence map of and the common characteristics of the mystical materials are also established. We then illustrate that the properties of these mystical materials may still be distinguishable by alternative indentation techniques, for example, a film indentation analysis (Zhao et al. 2006a) and an improved spherical indentation technique (Zhao et al. 2006a), which are suitable for specimens with finite thickness and bulk materials, respectively.

Challenging the Uniqueness of Indentation Load-Displacement Curve vs. Material Property

Most indentation techniques, the sharp indentation analysis, the spherical indentation analysis, the film indentation analysis, etc., in essence, require numerical analyses to correlate various shape factors of the P-δ curve with the specimen elastoplastic properties. In doing so, a critical theoretical question emerges: is there a one-to-one correspondence between indentation load-displacement curves (for loading and/or unloading) and material properties (E, ν, σ_y, n)? The uniqueness of the solution of the reverse analysis is the key verification for all indentation analyses – although some of those methods are now widely used in practice and cited in literature, unfortunately, the uniqueness of their solutions has been rarely challenged.

The fundamental question is, does a set of mystical materials which will yield indistinguishable indentation load-displacement curves for not only one particular indenter angle, but also another indenter angle exist? If this is true, then the dual (or plural) indenter method, regardless of the detail of the theory, cannot be used to distinguish these mystical materials. Such a fundamental question is not only the basis for the dual (or plural) sharp indenter method but also the foundation of the spherical indentation and film indentation techniques, as well as most indentation analyses which rely on the load-displacement curves.

In what follows, we will first present a simple and explicit technique to derive special sets of materials (with different elastoplastic properties) that lead to the same loading curves during sharp indentation when different indenter angles are used. Next, we show another technique to derive special sets of materials that yield almost same loading and unloading curves for a given indenter angle. We then extend our analysis to predict the mystical materials that have indistinguishable loading and unloading curves when different sharp indenters are used. Consequently, many of the previously established indentation analyses would fail to distinguish these materials. The existence range, trend, and special features of the mystical materials are discussed. We also show that these mystical materials may still be distinguished by using the improved spherical indentation and film indentation techniques.

Computation Method

In this chapter, the relationships between indentation responses, material properties, and indenter geometries are established from extensive finite element analyses. FEM calculations are performed using the commercial code. The rigid contact surface option is used to simulate the rigid indenter, and the option for finite deformation and strain is employed. A typical mesh for the axisymmetric indentation model comprises about 10,000 4-node elements with reduced integration. The Coulomb's friction law is used between contact surfaces, and the friction coefficient is taken to be 0.15 (Bowden and Tabor 1950), which is a minor factor for indentation (Mesarovic and Fleck 1999; Cheng and Cheng 2004) as long as this value is relatively small. The strain gradient effect is ignored by assuming that the indentation

Fig. 1 The relationship between C/σ_R and $\overline{E}/\sigma_R$ as n is varied, for $\alpha = 70.3$. The numerical results (symbols) are shown with both elastic and rigid plastic limits, and the empirical fitting function incorporating these limits is given in Eq. 6 (which can be extended to other angles) (Chen et al. 2007)
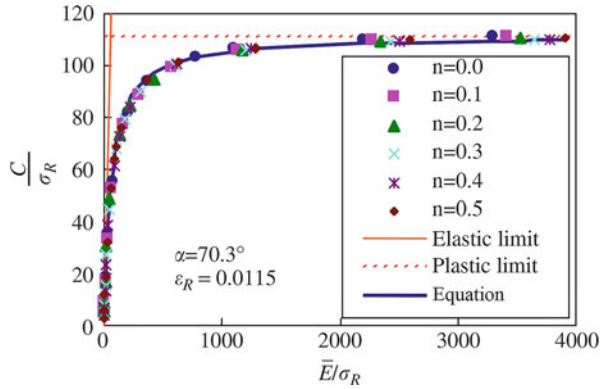
depth is sufficiently deep so that the continuum mechanics still applies to the bulk specimen. In addition, the strain rate effect is also ignored. In order to obtain both complete and robust numerical results, the material parameters are varied over a large range to cover essentially all engineering materials with $\overline{E}/\sigma_R = 3 - 3900$ and $n = 0$–0.5, where $\overline{E}$ is the plane-strain modulus and σ_R is the representative stress, see (Ogasawara et al. 2005, 2007a) for details. And, for the same reason, a large indenter angle range is also used, from 60° to 80°, which covers most of the angle range used in literature. To be consistent with most literature, Poisson's ratio is fixed at 0.3.

Determine Special Materials with Same Loading Curves for Dual Sharp Indenters

A Simple Relationship Between the Loading Curvature and Material Properties

When a sharp indenter is penetrating a bulk specimen, the loading P-δ relationship is always quadratic, i.e., $P = C\delta^2$. Therefore, two materials must have the same loading curvature C in order to have the same loading P-δ curve. A simple relationship, not a high-order fitting polynomial function, between C and $\overline{E}/\sigma_R$ must be established on a physical basis.

Note that the specimen is essentially elastic when the variable $\overline{E}/\sigma_R => 0$, whereas the material approaches to rigid plastic when $\overline{E}/\sigma_R => \infty$ – the functional form $\prod(\overline{E}/\sigma_R)$ should incorporate the limits of both mechanisms, such that it remains valid for all materials regardless of the range of data used for fitting. In the representative case of $\alpha = 70.3$ (Fig. 1), both of the elastic and rigid plastic limits can be well defined:

(a) When $\overline{E}/\sigma_R => 0$(elastic), $C/\sigma_R = \prod(\overline{E}/\sigma_R)$ varies linearly with $\overline{E}/\sigma_R$:

$$\frac{C}{\sigma_R} = m_e \frac{\overline{E}}{\sigma_R} \text{ as } \overline{E}/\sigma_R => 0, \tag{2}$$

where m_e can be derived from the classic solution of indentation on elastic materials (Sneddon 1965), and it agrees well with FEM calculations (Ogasawara et al. 2006):

$$m_e = \frac{2\gamma \tan \alpha}{\pi}. \tag{3}$$

(b) When $\overline{E}/\sigma_R => \infty$(rigid plastic), C/σ_R approaches a constant:

$$\frac{C}{\sigma_R} = m_p \text{ as } \overline{E}/\sigma_R => \infty, \tag{4}$$

where m_p is the rigid plastic limit of conical indentation into a material that obeys the Mises yield criterion.

$$m_p = 13.2 \tan^2\alpha + 6.18 \tan \alpha - 8.54 \tag{5}$$

for $50^\circ \le \alpha \le 80^\circ$. m_p is equal to 112.1 for the Berkovich indenter. In view of the importance of these two limits, we have proposed a very simple empirical form of $\prod \left(\overline{E}/\sigma_R \right)$ to incorporate both limits (Ogasawara et al. 2006, 2007a):

$$\prod = \frac{C}{\sigma_R} = \left(\frac{1}{m_e \frac{\overline{E}}{\sigma_R}} + \frac{1}{m_p} \right)^{-1}, \tag{6}$$

from which the representative stress can be obtained as $\sigma_R = m_e C \overline{E} / m_p \left(m_e \overline{E} - C \right)$ without iteration. The above equation not only incorporates the elastic and plastic limits (thus having physical meaning and wider range of application), but it also involves no fitting parameter if m_p could be solved analytically.

Special Materials with Same Loading Curvature for Dual Sharp Indenters

With the simple Eq. 6 relating C and material properties, it is now possible to explicitly derive material combinations that have the same loading curvature. First consider the case with one indenter (#A) whose half-apex angle is fixed: once α^A is specified, its related elastic limit m_e^A, rigid plastic limit m_p^A, and representative strain $\varepsilon_R^A = 0.0319 \cot \alpha^A$ can be fixed. For two materials, #1 with elastoplastic property (E_1, σ_{y1}, n_1) and #2 with elastoplastic property (E_2, σ_{y2}, n_2), to have the same loading P-δ curve they must satisfy

$$C_1^A = \frac{m_e^A m_p^A \overline{E}_1}{m_e^A \frac{\overline{E}_1}{\sigma_{R1}^A} + m_p^A} = C_2^A = \frac{m_e^A m_p^A \overline{E}_2}{m_e^A \frac{\overline{E}_2}{\sigma_{R2}^A} + m_p^A}, \tag{7}$$

where the representative stresses are

$$\sigma_{R1}^A = R_1 \left(2\frac{\sigma_{R1}^A}{E_1} + 2\varepsilon_R^A \right)^{n_1} \tag{8}$$

and

$$\sigma_{R2}^A = R_2 \left(2\frac{\sigma_{R2}^A}{E_2} + 2\varepsilon_R^A \right)^{n_2} \tag{9}$$

respectively, and they need to satisfy

$$\frac{1}{\sigma_{R2}^A} = \frac{1}{\sigma_{R1}^A} + \frac{m_p^A}{m_e^A} \left(\frac{1}{\overline{E}_1} - \frac{1}{\overline{E}_2} \right). \tag{10}$$

Similarly, for another sharp indenter (#B) with a different angle α^B, its elastic limit is m_e^B, rigid plastic limit is m_p^B, and representative strain is ε_R^B. If the two materials will again have the same loading curvature, their representative stresses need to satisfy

$$\frac{1}{\sigma_{R2}^B} = \frac{1}{\sigma_{R1}^B} + \frac{m_p^B}{m_e^B} \left(\frac{1}{\overline{E}_1} - \frac{1}{\overline{E}_2} \right) \tag{11}$$

with

$$\sigma_{R1}^B = R_1 \left(2\frac{\sigma_{R1}^B}{E_1} + 2\varepsilon_R^B \right)^{n_1} \tag{12}$$

and

$$\sigma_{R2}^B = R_2 \left(2\frac{\sigma_{R2}^B}{E_2} + 2\varepsilon_R^B \right)^{n_2}. \tag{13}$$

The procedure of deriving two materials with different elastoplastic properties yet with the same loading curvature (for both indenters #A and #B) can be concluded as

(a) Choose any E_1 and E_2 that are different (with fixed $\nu_1 = \nu_2 = 0.3$).
(b) Choose any value of σ_{y1} and n_1, and derive $R_1 = \sigma_{y1} (E_1/\sigma_{y1})^{n_1}$.
(c) Calculate σ_{R1}^A from Eq. 8 and solve for σ_{R2}^A from Eq. 10.
(d) Obtain one flow stress-total strain pair of the uniaxial stress-strain curve for material #2 as $\sigma_2^A = \sigma_{R2}^A$ and $\varepsilon_2^A = 2\varepsilon_R^A + 2\sigma_{R2}^A/E_2$.
(e) Calculate σ_{R1}^B from Eq. 12 and solve for σ_{R2}^B from Eq. 13.
(f) Obtain another flow stress-total strain pair for material #2 as $\sigma_2^B = \sigma_{R2}^B$ and $\varepsilon_2^B = 2\varepsilon_R^B + 2\sigma_{R2}^B/E_2$.

(g) From both flow stress-total strain pairs, solve $n_2 = \ln\left(\sigma_2^A/\sigma_2^B\right)/\ln\left(\varepsilon_2^A/\varepsilon_2^B\right)$, $R_2 = \sigma_2^A/\left(\varepsilon_2^A\right)^{n_2}$, and $\sigma_{y2} = \left((E_2)^{n_2/(n_2-1)}/(R_2)^{1/(n_2-1)}\right)$. Finally, from the numerical indentation test, confirm that $C_1^A = C_2^A$ and $C_1^B = C_2^B$.

Therefore, for any given material #1 with elastoplastic property (E_1, σ_{y1}, n_1), we can explicitly derive a special material #2 with elastoplastic property (E_2, σ_{y2}, n_2) such that they not only yield the same loading curvature when indenter #A is used but also have the same loading curvature when indenter #B is used. There are infinite numbers of such special siblings. The procedure outlined above can be readily extended to identify materials with indistinguishable indentation loading P-δ curves for three different sharp indenters (#A, #B, #C).

An example of the set of special materials is given in Fig. 2: for the five materials (mat1–mat5) that have distinct elastoplastic properties, their uniaxial stress-strain relationships are given in the inset of Fig. 2. These materials not only have the same loading curvature for the Berkovich indenter but are also the same when $\alpha=63.14°$, 75.79°, and 80.0° are used; moreover, for any indenter angle between 63.14° and 80°, their loading curvatures are also the same. From Eqs. 10 and 11, if $\overline{E}_1 > \overline{E}_2$ then $\sigma_{R1}^A < \sigma_{R2}^A$ and $\sigma_{R1}^B < \sigma_{R2}^B$ – this can be verified from the inset where for the special sets of materials, the ones with larger moduli have smaller representative stresses. Moreover, when $\alpha^B > \alpha^A$, we have $\varepsilon_R^B < \varepsilon_R^A$ and $m_p^B/m_e^B < m_p^A/m_e^A$. Therefore, for a pair of such special materials, if $\overline{E}_1 > \overline{E}_2$, the difference between σ_1^B and σ_2^B is larger than that of σ_1^A and σ_2^A, and thus $n_1 > n_2$ and $\sigma_{y1} < \sigma_{y2}$, all can be verified from Fig. 2. In this case, the uniaxial stress-strain curves of these special two materials must intersect outside ε_2^A.

From Fig. 2, during unloading the contact stiffness (and thus unloading work) of these special materials are different, which means that if their Young's moduli are known (with a fixed ν), their plastic properties (σ_y, n) can still be uniquely determined from the loading curvature by using the dual (or plural) indenter method, under the important premise that the two indenter angles are distinct enough such that the two determined total strains ε_2^A and ε_2^B are separated sufficiently apart (to ensure numerical accuracy) (Ogasawara et al. 2006).

Determine Special Materials with Same Loading and Unloading Curves for one Conical Indenter

Relating the Unloading Work with Material Properties

While the normalized C (or equivalently, loading work W_t) is the only shape factor during loading, in principle, there are three shape factors for unloading: the normalized δ_f, contact stiffness S, and unloading work W_e. However, only one of them is completely independent; this is because the curvature of the unloading curve of conical indentation (c.f. Fig. 2) is usually very small (except by the end of the unloading process). Therefore, if either one of the variables (δ_f, S, W_e) is
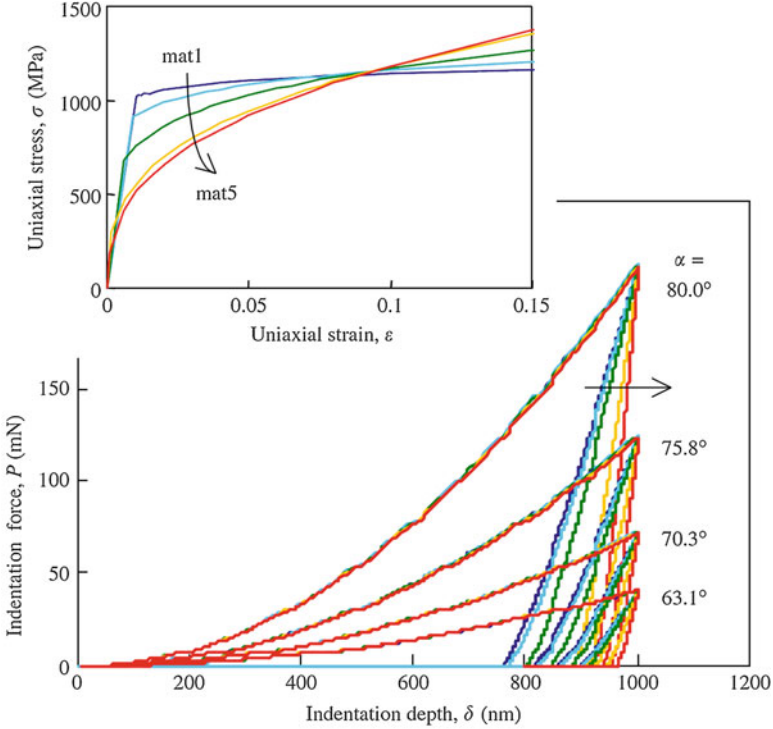
Fig. 2 A set of special materials with same loading curvatures when different indenter angles (63.14°, 70.3°, 75.79°, 80.0°) are used. The five materials have elastoplastic properties (E, σ_y, n) as mat1 (100 GPa, 1022 MPa, 0.05), mat2 (105.0GPa, 911.4 MPa, 0.10), mat3 (120.0 GPa, 678.3 MPa, 0.19), mat4 (200.0 GPa, 299.8 MPa, 0.33), and mat5 (300.0 GPa, 185.0 MPa, 0.37), respectively. The uniaxial stress-strain curves of these special materials are given in the inset on the top-left corner (Chen et al. 2007)

known, from the unloading triangle (plus the knowledge of C), the other two shape factors can be approximately derived. In order to make the best overall matching of the unloading curves, we take the normalized unloading work W_e as the governing unloading shape factor.

Since the unloading work depends on both the contact stiffness (which is related with $\overline{E}$) and the maximum load (which is related with C), a new representative stress for unloading, σ_r, is sought such that the normalized unloading work is related with both $\overline{E}$ and C, but is essentially independent of n. A representative example is given in Fig. 3 for the Berkovich indenter where the unloading work is fitted by

$$\frac{\delta^3 \sigma_r}{W_e} = \lambda_1 \frac{\overline{E}}{\sigma_r} + \lambda_0 \tag{14}$$

Fig. 3 The relationship between $\delta^3\sigma_r/W_e$ and $\overline{E}/\sigma_r$ for plastic materials, with $\overline{E}/\sigma_r > 30$ or so (Chen et al. 2007)
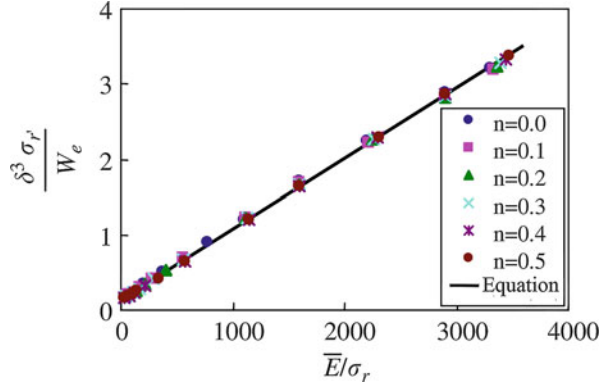
for plastic material with $\overline{E}/\sigma_r > 30$. $\lambda_1 = 0.0009322$ and $\lambda_0 = 0.1402$ for $\alpha = 70.3°$, and they take different values for other α. The representative stress σ_r is given by

$$\sigma_r = R\left(1.3\frac{\sigma_r}{E} + 2.6\varepsilon_R\right)^n, \tag{15}$$

which is valid for α between 60° and 80°. The simple functional forms derived in this section permit an explicit derivation of special materials with almost same unloading work, elaborated below.

Special Materials with Same Loading and Unloading Curves for a Sharp Indenter

Although Alkorta et al. (2005) have determined special materials with the same loading and unloading curves for one particular indenter, here we report an improved procedure to explicitly derive such materials, which also sets a part of the basis for finding the mystical materials. Based on Eq. 14, for a given indenter #A with half-apex angle α^A and two materials with elastoplastic properties (E_1, σ_{y1}, n_1) and (E_2, σ_{y2}, n_2), if they are to have the same unloading work, they need to satisfy

$$\frac{\delta^3}{W_{e1}^A} = \lambda_1\frac{\overline{E}_1}{(\sigma_{r1}^A)^2} + \lambda_0\frac{1}{\sigma_{r1}^A} = \frac{\delta^3}{W_{e2}^A} = \lambda_1\frac{\overline{E}_2}{(\sigma_{r2}^A)^2} + \lambda_0\frac{1}{\sigma_{r2}^A}, \tag{16}$$

where $\varepsilon_R^A = 0.0319\cot\alpha^A$, and $\sigma_{r1}^A = R_1\left(1.3\sigma_{r1}/E_1 + 2.6\varepsilon_R^A\right)^{n_1}$ and $\sigma_{r2}^A = R_2\left(1.3\sigma_{r2}/E_2 + 2.6\varepsilon_R^A\right)^{n_2}$ are the unloading representative stresses for materials #1 and #2 of indenter #A, respectively. Thus,

$$\sigma_{r2}^A = \frac{\lambda_0 + \sqrt{\lambda_0^2 + 4\left(\lambda_1 \frac{\overline{E}_1}{(\sigma_{r1}^A)^2} + \lambda_0 \frac{1}{\sigma_{r1}^A}\right)(\lambda_1 \overline{E}_2)}}{2\left(\lambda_1 \frac{\overline{E}_1}{(\sigma_{r1}^A)^2} + \lambda_0 \frac{1}{\sigma_{r1}^A}\right)}. \tag{17}$$

Therefore, the procedure of deriving two materials with different elastoplastic properties yet with almost the same loading and unloading curves (for indenter #A) can be concluded as

(a) Choose any E_1 and E_2 that are different (with fixed $\nu_1 = \nu_2 = 0.3$).
(b) Choose any value of σ_{y1} and n_1 (as long as material #1 remains sufficiently plastic), and derive $R_1 = \sigma_{y1}(E_1/\sigma_{y1})^{n_1}$.
(c) Calculate σ_{R1}^A from Eq. 8 and solve for σ_{R2}^A from Eq. 10.
(d) Obtain a flow stress-total strain pair of the uniaxial stress-strain curve for material #2 as $\sigma_2^A = \sigma_{R2}^A$ and $\varepsilon_2^A = 2\varepsilon_R^A + 2\sigma_{R2}^A/E_2$.
(e) Calculate σ_{R1}^A from Eq. 15 and solve for σ_{R2}^A from Eq. 17.
(f) Obtain another flow stress-total strain pair for material #2 as $\sigma_2^a = \sigma_{r2}^A$ and $\varepsilon_2^a = 2.6\varepsilon_R^A + 1.3\sigma_{r2}^A/E_2$.
(g) From the stress-strain pairs, solve $n_2 = \ln\left(\sigma_2^A/\sigma_2^a\right)/\ln\left(\varepsilon_2^A/\varepsilon_2^a\right)$, $R_2 = \sigma_2^A/(\varepsilon_2^A)^{n_2}$, and $\sigma_{y2} = \left((E_2)^{n_2/(n_2-1)}/(R_2)^{1/(n_2-1)}\right)$. Finally, carry out a numerical test to verify that indeed $C_1^A = C_2^A$ and $W_{e1}^A = W_{e2}^A$.

Therefore, for any material #1 with (E_1, σ_{y1}, n_1), a special material #2 with (E_2, σ_{y2}, n_2) can be explicitly derived such that they yield indistinguishable loading and unloading curves for a given conical indenter. There are infinite sets of such special materials, and identification of these is no longer based on "trial and error." An example of such is given in Fig. 4, where the effectiveness of the proposed approach is validated (with the difference of C and W_e less than 0.5% – such very small difference is due to the error of fitting functions and numerical solutions which is inevitable). This pair of material cannot be distinguished by only using the Berkovich indenter, yet their P-δ curves may become separable with other distinct indenter angles.

According to Eq. 16, if $\overline{E}_1 > \overline{E}_2$ it can be shown that $\sigma_{r1}^A > \sigma_{r2}^A$, whereas from Eq. 10, $\sigma_{R1}^A > \sigma_{R2}^A$. For most plastic materials, the representative strain is much larger than yield strain; thus, the two identified total strains satisfy $\varepsilon_2^a > \varepsilon_2^A$ – this implies that for a pair of special materials, if $\overline{E}_1 > \overline{E}_2$, then $n_1 > n_2$ and $\sigma_{y1} < \sigma_{y2}$; in addition, the stress-strain curves of material #1 and #2 must intersect between ε_2^a and ε_2^A. Thus, if two special materials also have the same loading and unloading curves for indenter #B, their intersection point must also be placed between ε_2^b and ε_2^B; this is only possible when the difference between α^A and α^B is not too extreme (since both ε_R^A and ε_R^B vary as indenter angle changes, and such variation is more prominent for sharper angles). That is, the mystical materials, if they exist, should be valid within a specified range of indenter angles – more discussions are given in the next subsection.
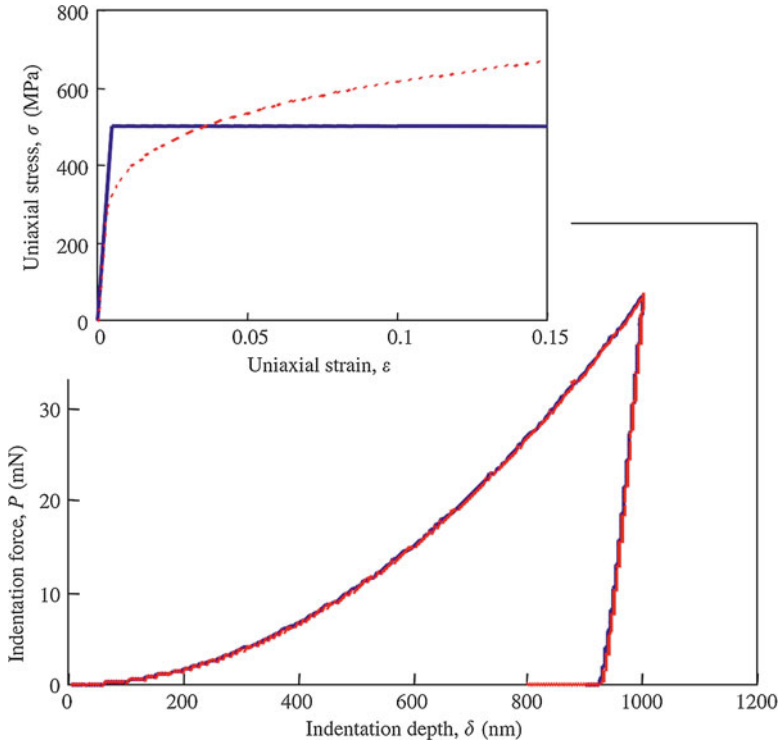
Fig. 4 A pair of special materials with indistinguishable loading and unloading curves when $\alpha=70.3$. The black solid curve represents the material with $(E, \sigma_y, n) = (100.0\,\text{GPa}, 500.0\,\text{MPa}, 0.0)$, and the red dash curve represents the material with $(E, \sigma_y, n) = (110.0\,\text{GPa}, 295.0\,\text{MPa}, 0.2)$. The uniaxial stress-strain curves of these special materials are given in the inset on the top-left corner (Chen et al. 2007)

Determine Mystical Materials with Same Loading and Unloading Curve for Dual Indenters

Weak-Form Mystical Materials and Their Possible Existence

In most previous dual (or plural) indentation approaches with Poisson's ratio fixed, the material elastic modulus is first obtained from the unloading curve of one particular indenter (e.g., $\alpha=70.3°$). Next, the representative stress-based approach is used to determine two (or more) flow stress-total strain points on the uniaxial stress-strain curve, by utilizing the loading curvatures obtained from dual (or plural) sharp indenters. Therefore, if we could identify a pair of special materials with elastoplastic properties (E_1, σ_{y1}, n_1) and (E_2, σ_{y2}, n_2) (their Poisson's ratio $v_1 = v_2 = 0.3$), such that they yield indistinguishable loading and unloading P-δ curves for indenter #A (e.g., $\alpha=70.3°$), and also almost identical loading curvature

for another indenter #B, then the conventional dual (or plural) indentation analysis would fail since it cannot promise unique solution. This pair of special materials, which does not require their unloading works to match for indenter #B, may be termed as the weak-form mystical materials.

Meanwhile note that in a displacement-controlled experiment where the maximum penetration is fixed, if $C_1^A = C_2^A$ and $C_1^B = C_2^B$, then the maximum indentation load for these two materials are also the same. Thus, to make their unloading works to match for indenter #A $\left(W_{e1}^A = W_{e2}^A\right)$, their contact stiffness must be fairly close $\left(S_1^A \approx S_2^A\right)$, the two materials must have close Young's moduli $\left(\overline{E}_1 \approx \overline{E}_2\right)$, and this also implies their unloading works for indenter #B must also be very close $\left(W_{e1}^B \approx W_{e2}^B\right)$. Thus, the weak-form mystical materials are very close to the mystical materials we are looking for.

What general properties must the weak-form mystical materials satisfy (assuming they are sufficiently plastic such that Eq. 14 applies)? Since these materials must be a subset of the special materials derived from the above procedures, therefore, with $(\alpha^B > \alpha^A)$, if $\left(\overline{E}_1 < \overline{E}_2\right)$, the two mystical materials must satisfy $n_1 < n_2$ and $\sigma_{y1} > \sigma_{y2}$; moreover, the uniaxial stress-strain curves of these two materials must intersect outside $2\varepsilon_R^A$ but inside $2.6\varepsilon_R^A$. A schematic showing of the relative status of the two mystical materials is given in Fig. 5a. Since these two candidates need to intersect within a relatively small region, this implies that the mystical materials would only exist for a specified range of indenter angle (with $\alpha^B > \alpha^A$) and material properties. For the current case, the difference between α^B and α^A cannot be too extreme, and the materials need to be sufficiently plastic (with large E_1/σ_{y1} and E_2/σ_{y2}) so as to leave enough possible space for materials #1 and #2 to intersect within the desired region.

Next, we consider the case with $\alpha^B < \alpha^A$, but the difference is not so much such that $2\varepsilon_R^A < 2\varepsilon_R^B < 2.6\varepsilon_R^A$. If $\overline{E}_1 < \overline{E}_2$, then from the above procedures, $\sigma_{R1}^A = \sigma_1^A > \sigma_{R2}^A = \sigma_2^A$ and $\sigma_{R1}^B = \sigma_1^B > \sigma_{R2}^B = \sigma_2^B$; since $m_p^A/m_e^A > m_p^B/m_e^B$, so the difference between σ_1^A and σ_2^A is larger than that of σ_1^B and σ_2^B; moreover, the unloading representative stresses satisfy $\sigma_{r1}^A = \sigma_1^a > \sigma_{r2}^A = \sigma_2^a$. All these features lead to $n_1 < n_2$ and $\sigma_{y1} > \sigma_{y2}$, and a possible solution for the mystical pair #1 and #2 is sketched in Fig. 5b. In this case, the uniaxial stress-strain curves of these two materials must intersect between $2\varepsilon_R^B$ and $2.6\varepsilon_R^A$, and such range is even narrower than that in Fig. 5a. That is, the mystical materials may exist in a small space of material properties and indenter angles; nevertheless, such solution is possible.

When α^B is much smaller than α^A such that $2\varepsilon_R^B > 2.6\varepsilon_R^B$, all the relative magnitudes of the representative stresses discussed in the last paragraph still hold, except that now those related with $2\varepsilon_R^B$ are moved to the right side of those related with $2.6\varepsilon_R^A$ – according to the new schematic in Fig. 5c, it is impossible to find a solution for the mystical material. This implies that if the indenter #A is the Berkovich tip, the indenter #B must be larger than about $64.88°$ such that the mystical materials may exist according to Fig. 5a, b. Similarly, if #B is taken to be the Berkovich tip (since the weak-form mystical material is very close to the desired mystical material), then #A must be smaller than $74.50°$. Therefore, rigorously

Fig. 5 Schematics of possible solutions of a pair of weak-form plastic mystical materials; assuming $\overline{E}_1 < \overline{E}_2$, then $n_1 < n_2$ and $\sigma_{y1} > \sigma_{y2}$. The indenter angle $A(\alpha^A)$ is fixed (which equals to 70.3° in many existing dual indenter techniques). (**a**) When $\alpha^B > \alpha^A$ solution is possible. (**b**) When $\alpha^B < \alpha^A$ but $2\varepsilon_R^B < 2.6\varepsilon_R^A$, solution is possible. (**c**) When $\alpha^B < \alpha^A$ and the difference between these two angles is large such that $2\varepsilon_R^B > 2.6\varepsilon_R^A$, rigorous solution is not possible (Chen et al. 2007)
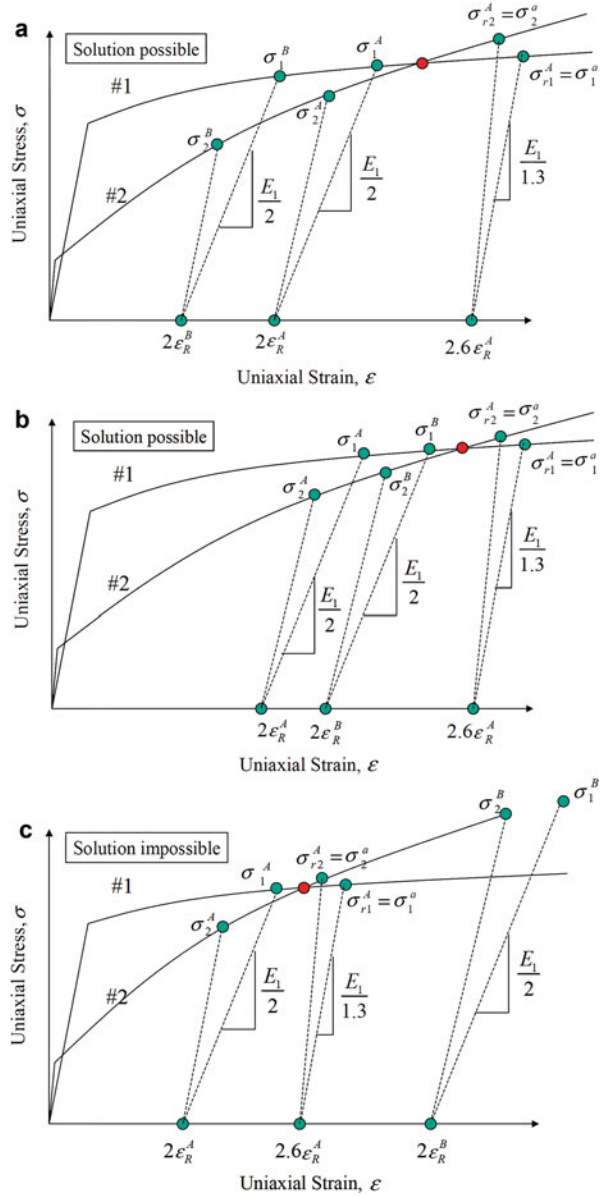
speaking, under the premise that Poisson's ratio is always fixed at 0.3, if a Berkovich tip is used in the dual indenter method, the mystical materials would only be possible if the other indenter angle is between 64.88° and 74.50°. Moreover, such mystical materials need to be relatively plastic.

Fig. 6 The schematic of the possible existence of the mystical materials and relevant indenter angle ranges – they correspond to the plateaus on the multidimensional surface of the shape factors of the P-δ curves (Chen et al. 2007)
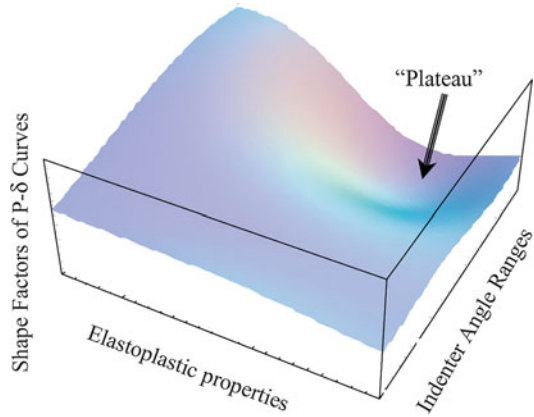
In a short summary, there is no pair of mystical materials that would be applicable to arbitrary large range of indenter angles, and only for limited material space-indenter angle combinations can the mystical siblings be found – this is part of the reason the mystical materials were not discovered in the past. The current problem of finding the mystical materials is analogous to a multivariable problem (Fig. 6), where the indentation shape factors (the general z-axis) are related with the material elastoplastic properties (the general x-axis) and indenter angle ranges (the general y-axis) through a multidimensional surface. On such surface, the slope may not be large and distinct everywhere, and small regions that are relatively flat may exist, as sketched in Fig. 6. The mystical materials and the relevant indenter angle ranges would correspond to such plateaus (with zero or almost zero slope) of the multidimensional surface – although these plateaus are small compared with the entire parameter space, they may still exist and thus have important theoretical value for probing the uniqueness of indentation analysis. The search of such plateaus is elaborated next.

Search for Mystical Materials with Fixed Poisson's Ratio

In most literature of indentation analysis, Poisson's ratio was fixed by neglecting its influence. In order to challenge the basis of the uniqueness solution and be consistent with the literature, a fixed $\nu = 0.3$ is used in most part of this chapter.

For a given pair of indenters #A and #B, and a given material #1 which is sufficiently plastic, in order to identify the weak-form mystical siblings, Eqs. 10, 11, and 17 need to be satisfied rigorously, from which σ_{R2}^{A}, σ_{R2}^{B}, and σ_{r2}^{A} can be derived (with any specified $\overline{E}_2$), respectively. Unfortunately, the only solution that rigorously satisfies all these equations is exactly material #1. On the other hand, note that there are no perfect finite element solution and numerical fitting, and all numerical results are subject to small error. It is then acceptable if small errors are added to fitting functions Eqs. 10, 11, and 17, such that the resulting

loading/unloading P-δ curves of material #2 would be indistinguishable to that of material #1, with the difference between their shape factors below several percent – such small perturbation is also inevitable in the data measured from any real experiment. Another advantage is that, when small perturbation to the shape function is allowed, the existence range of the mystical material is significantly enlarged, in terms of both the material property and indenter angle space. In essence, although it is difficult to search for perfect plateaus (with exactly zero slope) on the multidimensional surface describing the indentation shape factors, it is possible to search for plateaus with slopes that are very close to zero through a numerical algorithm – the results are still the indistinguishable mystical materials given the inevitable small perturbations in numerical and experimental indentation tests. The search process is also relatively straightforward since the simple and explicit formulations of the primary shape factors of loading/unloading P-δ curves are established earlier. Of course, with Poisson's ratio fixed at 0.3, such identification procedure is no longer explicit.

The numerical search process is the following (with fixed $\nu_1 = \nu_2 = 0.3$):

(a) Choose any E_1 and α^A (e.g., the Berkovich tip).
(b) Choose any initial value of α^B and then iterate such that its difference with respect to α^A is increased.
(c) Choose initial values of n_1 and σ_{y1} and then iterate, preferably in the plastic material range.
(d) Choose an initial value of E_2 which is at least 5% different than E_1 and then iterate, such that the difference could become bigger. This ensures that the initial guesses of material #1 and #2 are sufficiently different.
(e) From Eqs. 10, 11, and 17, solve for σ_{R2}^A, σ_{R2}^B, and σ_{r2}^A.
(f) Give small errors (few percent) to Eqs. 10, 11, and 17. For example, if we wish to increase σ_{R2}^A by ω times (e.g., ω=1.01 for a 1% error), then from Eq. 6 the new representative stress of material #2 that is related with loading for indenter #A becomes

$$\sigma_{R2-error}^A = \left(\frac{1}{\omega \sigma_{R2}^A} + \frac{m_p^A}{m_e^A} \frac{1}{\overline{E}_2} \left(\frac{1}{\omega} - 1 \right) \right)^{-1} \tag{18}$$

Similarly, when error is permitted, the two other representative stresses are

$$\sigma_{R2-error}^B = \left(\frac{1}{\omega \sigma_{R2}^B} + \frac{m_p^B}{m_e^B} \frac{1}{\overline{E}_2} \left(\frac{1}{\omega} - 1 \right) \right)^{-1} \tag{19}$$

and

$$\sigma^A_{R2-error} = \left(\lambda_0 + \sqrt{ \lambda_0^2 + 4\left(\frac{\lambda_1}{\omega} \frac{\overline{E}_2}{\left(\sigma^A_{r2}\right)^2} + \frac{\lambda_0}{\omega} \frac{1}{\sigma^A_{r2}} \right) \left(\lambda_1 \overline{E}_2 \right) } \right) \Big/ $$
$$\left(2\frac{\lambda_1}{\omega} \frac{\overline{E}_2}{\left(\sigma^A_{r2}\right)^2} + 2\frac{\lambda_0}{\omega} \frac{1}{\sigma^A_{r2}} \right), \tag{20}$$

respectively. Therefore, by plus or minus several percent of error, the upper and lower bounds of the error bars of σ^A_{R2}, σ^B_{R2}, and σ^A_{r2} can be derived – when the three error bars are combined, an error band can be formed.

(g) For all possible combinations of σ^A_{R2}, σ^B_{R2}, and σ^A_{r2} within the error band, the admissible solutions of material #2 are sought; since σ^A_{R2}, σ^B_{R2}, and σ^A_{r2} and E_2 must satisfy certain compatibility, only a small portion of the combinations within the error band could become candidate materials. For any admissible solution, their loading curvatures for indenters #A and #B can be estimated from Eq. 6, and their unloading work for indenter #A is obtained from Eq. 14; the results are then compared with that of material #1, and the more promising pairs with smaller errors are recorded along with the current indenter angle range. A candidate pair of mystical materials is found if the computed error is smaller than 2% for all shape factors.

(h) Iterate E_2.

(i) Iterate n_1 and σ_{y1}.

(j) Iterate α^B.

(k) Lastly, numerical indentation analyses are performed on the most promising candidate mystical material pairs using finite element simulations, to confirm that their loading and unloading curves are visually indistinguishable (i.e., the shape factors of their indentation curves are sufficiently close).

The existence range of the mystical materials is first explored through a series of maps in terms of materials space (E/σ_y, n). In Fig. 7a, b, the pairs of identified mystical materials are shown in line segments – both ends of each segment represent two mystical materials with different elastoplastic properties, yet they yield almost indistinguishable loading/unloading P-δ curves. For a given line segment, any sets of materials along the length of the segment are also mystical materials, and the most distinct mystical materials can be found at the ends of the longest segment. The area where the density of the segments is large indicates a possible gold mine of mystical materials.

For any given indenter angle range, the mystical materials can only exist within a certain region. As the difference between the dual indenters becomes larger, the existence range of the mystical material becomes smaller; moreover, the segments are shorter which also indicates the differences between their elastoplastic properties are smaller. Therefore, if a pair of extreme indenter angles (very sharp and very blunt) is used, the mystical materials do not exist (however, in experiments, the

Fig. 7 The existence maps of mystical materials for given indenter angle ranges, $(\alpha^A, \alpha^B) =$ **(a)** $(70.3°, 73°)$, **(b)** $(70.3°, 80°)$. Each segment links a pair of mystical materials within the material space $(E/\sigma_y, n)$. A gold mine of mystical materials is discovered when E/σ_y is about 100 and when n is small (Chen et al. 2007)
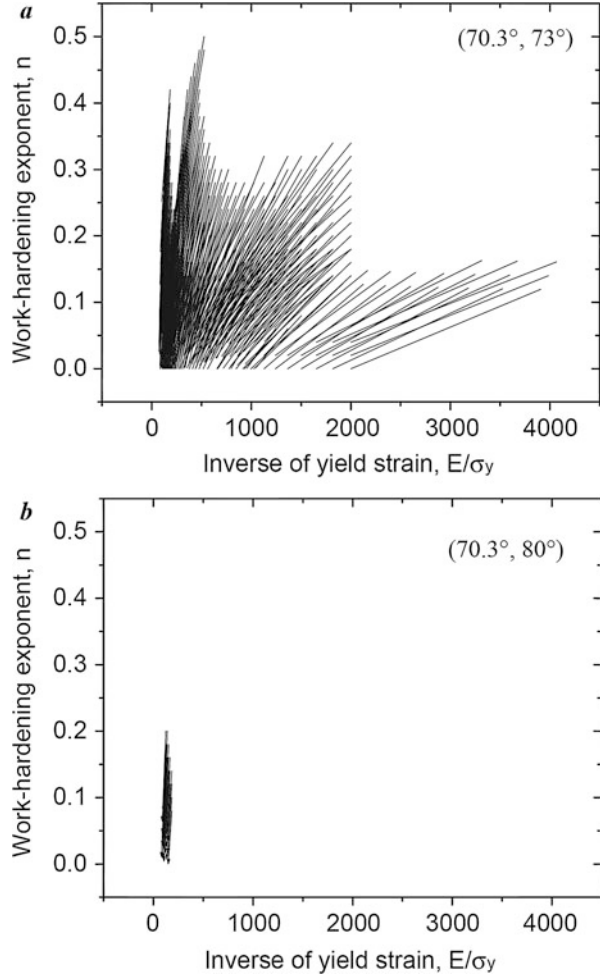
use of a pair of extreme sharp indenters is often impractical). In the examples illustrated in Fig. 7, $\alpha^A = 70.3°$ is always used because many previous studies rely on measuring the elastic modulus from a Berkovich indentation.

When the indenter angle range is relatively small, e.g., $(\alpha^A, \alpha^B) = (70.3°, 73°)$ (Fig. 7a), the mystical materials can be found in a large range, but notably for materials with smaller n. Quite a few of the more plastic mystical materials can exist with large differences of their elastoplastic properties. No mystical materials are available with both large n and large E/σ_y.

By contrary, when the indenter angle difference becomes larger, e.g., $(\alpha^A, \alpha^B) = (70.3°, 80°)$ (Fig. 7b), then the survival range of mystical materials are confined to the lower-left corner of the materials space map. Mystical materials become possible only for materials with $n = 0{-}0.2$ and $E/\sigma_y \approx 100$. Note that

if a pair of mystical materials is identified for a larger angle range, they are still mystical siblings for any subrange of indenter angles. Moreover, once a map for $(\alpha^A, \alpha^B) = (70.3°, 60°)$ is made and combined with Fig. 7b, their common elements are the extreme mystical materials that are effective when $(\alpha^A, \alpha^B) = (60°, 80°)$. Therefore, the materials with small n and with E/σ_y around 100 represent the gold mine around which many mystical materials can be identified. In fact, there are quite a few important engineering metals and alloys near this area, for example, Ti alloys, Ni alloys, Mg alloys, and high strength steel, in addition to a few ceramics and polymers (Ashby 1999) – extra care is needed for the measurement of their elastoplastic properties.

For the mystical materials identified in this section, with $\nu = 0.3$ but without knowing other information in advance, within the specified dual indenter angle range, their elastoplastic properties cannot be uniquely determined from the indentation analysis since their loading and unloading curves are indistinguishable.

Numerical indentation tests are carried out on these materials, and their $P\text{-}\delta$ curves are compared, which also reveal the characteristics of the mystical materials.

In Fig. 8a, for the indenter angle range $(\alpha^A, \alpha^B) = (70.3°, 74°)$, a pair of plastic mystical materials is chosen, with $E_1 = 100$ GPa, $\sigma_{y1} = 50$ MPa, $n_1 = 0.06$, and $E_2 = 110$ GPa, $\sigma_{y2} = 29.336$ MPa, and $n_2 = 0.17277$, respectively. Their uniaxial stress-strain curves are shown in the inset, and their corresponding indentation load-displacement curves are given. It is apparent that their indentation behaviors are almost identical (for both loading and unloading curves); specifically, the difference between C_1^A and C_2^A is about 2%, the difference between C_1^B and C_2^B is about 1%, and the difference between W_{e1}^A and W_{e2}^A is about 2%. The difference between W_{e1}^B and W_{e2}^B is about 4%; nevertheless, during the search of weak-form mystical materials, the matching criterion is not applied to the unloading curves with indenter #B. Note that when a larger indenter angle range is used, such as 63.14° and 75.79°, their $P\text{-}\delta$ curves become quite separable, and therefore it is still possible to use the established dual indenter method to measure the elastoplastic properties of these two materials with the wider indenter angle ranges.

In fact, a wider indenter angle separation also means that the two identified total strains are further apart, which also gives better numerical accuracy – a rule of thumb is that the two identified total strain should be separated by at least 30%, which is qualified for most plastic materials with indenter angles 63.14° and 75.79° (Ogasawara et al. 2007b), including the example in Fig. 8a. On the other hand, for the more elastic materials, the separation between the identified total strain points becomes smaller for a given indenter angle range. To ensure accuracy, a large indenter angle range $\Delta\alpha = |\alpha^A - \alpha^B|$ is recommended for more elastic materials with $E/\sigma_y < 100$ or so.

Figure 8b gives an intriguing example, which corresponds to $E_1 = 100$ GPa, $\sigma_{y1} = 872.47$ MPa, $n_1 = 0.0$, and $E_2 = 103.75$ GPa, $\sigma_{y2} = 715.61$ MPa, and $n_2 = 0.10663$. This pair of extreme mystical material leads to almost the same indentation loading/unloading behaviors when the indenter angle changes from 60° to 80°, which has reached the limit of the sharp indenter angles used in this study. Apparently, many existing dual (or plural) indentation methods in the literature
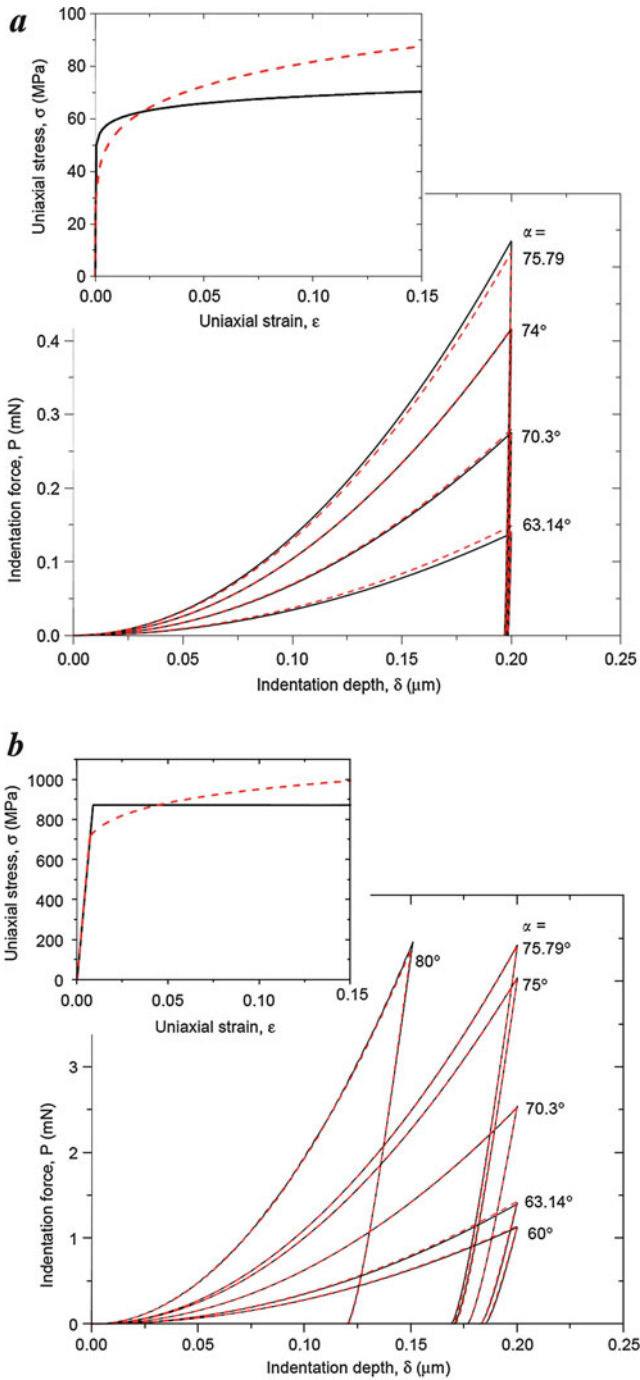
Fig. 8 (continued)

would fail to distinguish them, and more extreme indenters are needed. However, this is often not practical because without advanced knowledge, one could not predetermine what kind of $\Delta\alpha$ needs to be used in an experiment. Moreover, when extreme indenter angles are used, the measured hardness would differ by orders of magnitude, and new problems such as those associated with the resolution of the instrument, size effect, indenter tip alignment, and indentation cracking will emerge. In the next section, we will introduce how to use alternative methods to distinguish such extreme mystical pair.

For a pair of mystical materials near or inside the gold mine, their stress-strain curves tend to intersect around a total strain of 0.05. Moreover, if one material has a larger plane-strain modulus, then it always has larger work-hardening exponent and smaller yield stress.

Alternative Methods to Distinguish Mystical Materials

Improved Spherical Indentation

Spherical indenter has the unique advantage that with one penetration, the loading curvature is reduced as if the indenter angel becomes smaller. Since the mystical materials may be eventually distinguishable by a large $\Delta\alpha$, we only need to control the δ_{max} during spherical indentation. For that matter, the penetration depth has to be sufficiently deep and a few previous studies (e.g., Cao and Lu 2004) where $\delta_{max}/r = 0.1$) do not qualify; indeed, if δ_{max}/r is small (such as 0.1), the spherical indenter method still cannot distinguish the mystical materials because the effective $\Delta\alpha$ is small. Alternatively, in one of our works (Zhao et al. 2006b), an improved spherical indentation technique was proposed, which seems promising since $\delta_{max}/r = 0.3$, which mimics a very sharp indenter angle.

Figure 9a shows the spherical indentation result on the extreme mystical material pair derived from Fig. 8b. Initially, when the penetration is shallow, which is analogous to the blunter indenter angles, the two P-δ curves cannot be separated. However, when δ/r is larger than about 0.15, these two materials become distinguishable. Finally, at the maximum penetration, there is about 8% difference between their C. Although these two materials have very close contact stiffness and also C measured at $\delta/r = 0.13$, the relatively large difference at

Fig. 8 Representative case studies of mystical materials: the P-δ curves of mystical materials and the uniaxial σ-ε curves of mystical materials are given in inset on the top-left corner. (**a**) A pair of plastic mystical materials for $(\alpha^A, \alpha^B) = (70.3°, 74°)$, with $E_1 = 100$ GPa, $\sigma_{y1} = 50$ MPa, $n_1 = 0.06$ (solid curve), and $E_2 = 110$GPa, $\sigma_{y2} = 29.336$ MPa, $n_2 = 0.17277$ (dash curve). They can be distinguished when more different indenter angles are used. (**b**) A pair of extreme mystical materials with $E_1 = 100$ GPa, $\sigma_{y1} = 872.47$ MPa, $n_1 = 0.0$ (solid curve), and $E_2 = 103.75$ GPa, $\sigma_{y2} = 715.61$ MPa, $n_2 = 0.10663$ (dash curve). They cannot be effectively distinguished by indenter angles from $60°$ and $80°$ (Chen et al. 2007)

$\delta_{max}/r = 0.3$ is sufficient to make the spherical indentation technique work well. By following the reverse analysis procedure in Zhao et al. (2006b), the determined values are $E_1 = 102.5$ GPa, $\sigma_{y1} = 828.85$ MPa, $n_1 = 0.024$, and $E_2 = 106.34$ GPa, $\sigma_{y2} = 701.30$ MPa, and $n_2 = 0.108$, respectively. All errors (except that for n_1 cannot be counted since its true value is 0.0) are smaller than about 2% (except σ_{y1} which is about 5% and still within reasonable range). Finally, the identified uniaxial stress-strain curve from the reverse analysis of the improved spherical indentation method (Zhao et al. 2006b) is given in the inset, and its excellent capability of distinguishing the mystical material is justified. The improved spherical indentation technique proposed by Zhao et al. (2006b) only requires one simple indentation test, and thus it is convenient and reliable. This technique is therefore recommended for materials inside or near the gold mine of mystical materials.

Film Indentation

When an elastoplastic film with finite thickness is bonded to a rigid substrate, the increased conical penetration dramatically increases the loading curvature as if the sharp indenter angle is increased. Thus, the substrate effect provides an alternative way of obtaining extreme indenter angles to distinguish the mystical materials. We have proposed a theory, where the loading curvatures at the penetration of 1/3 and 2/3 of film thickness (h), along with the unloading work, are used to obtain the material elastoplastic properties from one fil indentation test (Zhao et al. 2006a). When this technique is applied to the extreme mystical materials (found in Fig. 8b, in Fig. 9b), it can be readily seen that their loading curvatures become quite different at $\delta_{max}/h = 2/3$, which is again sufficient to distinguish the extreme mystical pair although their loading curvatures at $\delta/r = 1/3$ are close. In addition, their unloading works are also different.

By following the reverse analysis described in Zhao et al. (2006a), finally the determined properties of the extreme pair of mystical materials are $E_1 = 97.5$ GPa, $\sigma_{y1} = 872.47$ MPa, $n_1 = 0.0$ and $E_2 = 103.75$ GPa, $\sigma_{y2} = 719.19$ MPa, $n_2 = 0.105$, respectively. All errors (except that for n_1 cannot be counted since its true value is 0.0) are smaller than 1.5% except E_1 which is only -2.5%. The identified uniaxial stress-strain curve from the film indentation technique (Zhao et al. 2006a) is given in the inset of Fig. 10, and it is demonstrated to be able to distinguish the mystical materials with high accuracy. Note that the advantage of the film indentation technique is that it may be applied to specimens with finite thickness; however, it also requires the testing platform (i.e., the substrate) to be sufficiently stiff and hard, which may not be practical in some cases (see Zhao et al. (2006a) for discussions). Nevertheless, it could be used as an alternative method to distinguish the mystical materials and is proven to work well.

In fact, from the error analysis of both the improved spherical indentation and film indentation methods (Zhao et al. 2006a, b), both techniques have the best accuracy for materials inside or near the gold mine of mystical materials, which make them complementary to the dual (or plural) sharp indentation analysis.
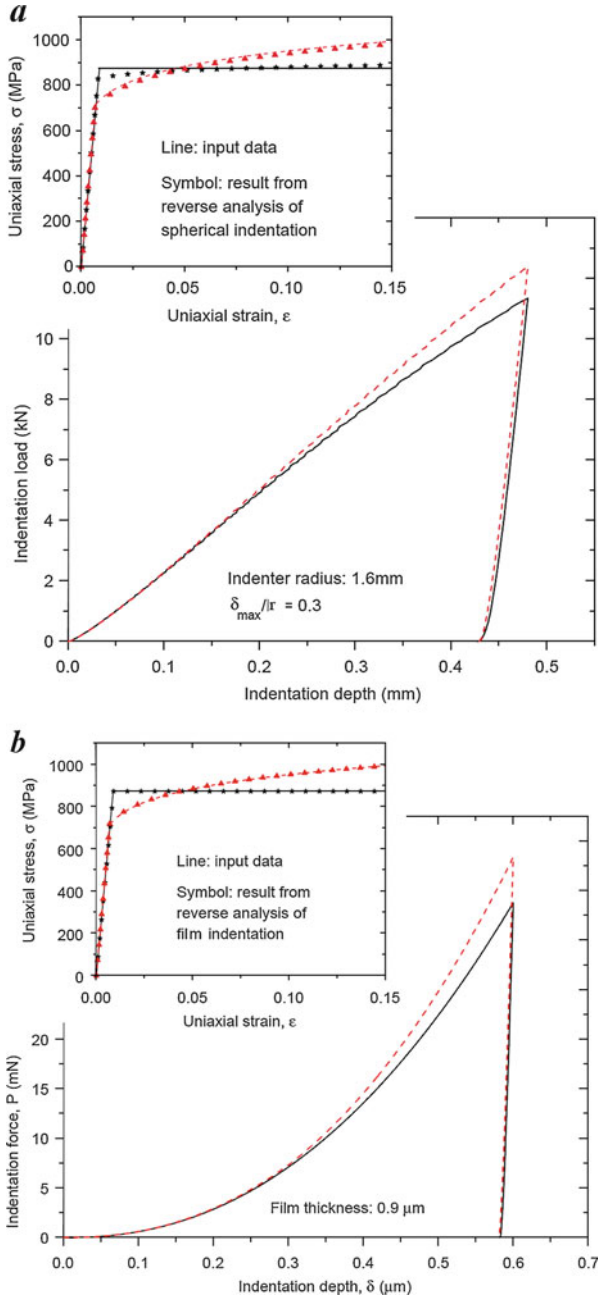
Fig. 9 The P-δ curves of two alternative indentation on the extreme mystical materials found in Fig. 8b. (**a**) Improved spherical indentation method (Zhao et al. 2006b). (**b**) Film indentation method (Zhao et al. 2006a). These methods can distinguish the extreme mystical materials – in the inset on top-left corner, the uniaxial stress-strain curves obtained from reverse analysis (symbols) are compared with the input (true) data and show excellent agreement (Chen et al. 2007)
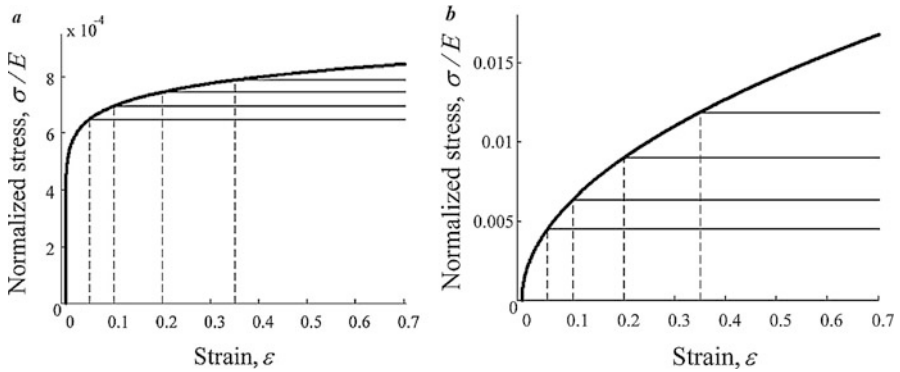
Fig. 10 Materials tailoring of two power-law materials (**a**) $E/\sigma_y = 2500$ and $n = 0.1$ and (**b**) $E/\sigma_y = 2500$ and $n = 0.5$. Thick lines are the uniaxial true stress-strain curves of untailored materials, and each thin line presents a modified material. Every modified material is defined as initially having the same constitutive curve with the original power-law material but becomes perfectly plastic beyond a bifurcation strain, ε_b. In the examples in both (**a**) and (**b**), ε_b equals 0.05, 0.1, 0.2, and 0.35 for the four tailored materials (Liu et al. 2009)

Detectable Strain Range of Indentation Test

The Critical Strain

When a sharp indenter penetrates a bulk specimen, the loading curvature C is only a function of the material elastoplastic; theoretically, any variation of the material constitutive relationship (the stress-strain curve) can, to a certain degree, cause C to deviate from its original value. However, there exists a critical strain beyond which tailoring material properties will no longer induce prominent variation to the indentation response (e.g., less than 1% deviation in the measured C). [The 1% threshold is set because it is a typical order-of-magnitude intrinsic error associated with numerical indentation analyses: below this critical level, one can hardly tell whether the difference is caused by material tailoring or by numerical error. Of course it could set a different threshold (e.g., 0.5%), but the critical strains derived from the new threshold are not going to be much different from the ones identified in this study, and the relevant conclusions still hold.] Therefore, indentation is limited to probing material elastoplastic properties within a particular strain range below critical, and the tailoring of the stress-strain curve beyond this range cannot be detected by indentation reverse analysis, leading to a non-unique solution.

To verify the existence of the critical strain and identify its dependence on material properties and indenter angles, without losing generality, we consider six representative power-law materials with $E/\sigma_y = 2500$, 1000, and 100 and $n = 0.1$ and 0.5. Two example stress-strain curves are given as thick lines in Fig. 10a, b. To tailor the constitutive relationship, one could choose any bifurcation strain $\varepsilon_b > \varepsilon_y$
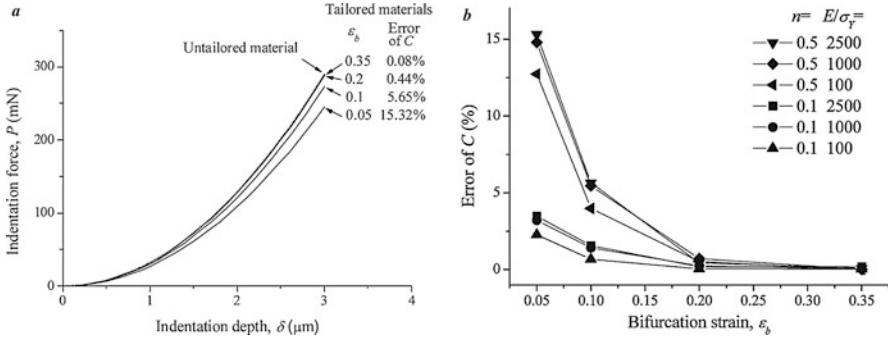
Fig. 11 (**a**) Indentation loading curves (with $\alpha=70.3°$) for a representative power-law material and four artificial materials tailored at different ε_b. The error of C is calculated as the difference of loading curvatures between each tailored materials and the untailored material. (**b**) The evolution of the error of C (with $\alpha=70.3°$) as a function of ε_b induced by material tailoring. A critical strain ε_c can be defined when the error of C falls below 1% (Liu et al. 2009)

and assign perfect plastic behavior after this point (the flat thin line in Fig. 10). In other words, the tailored stress-strain relationship becomes

$$
\begin{aligned}
\sigma &= E\varepsilon, \text{for } \varepsilon \leq \varepsilon_y \\
\sigma &= R\varepsilon^n, \text{for } \varepsilon_y \leq \varepsilon \leq \varepsilon_b \\
\sigma &= R\varepsilon_b^n = \text{constant, for } \varepsilon \geq \varepsilon_b.
\end{aligned}
\tag{21}
$$

Such a tailoring strategy provides a rough upper bound of the moderate modifications of the hardening function. For the selected cases shown in Fig. 10, ε_b equals 0.05, 0.1, 0.2, and 0.35 for the four modified materials. Upon indentation, the modified material will in principle show a different C from that of the original (unmodified) material, but S remains essentially unchanged since the elastic modulus is unaffected; thus, we only focus on the perturbation of C during loading.

Numerical indentation tests are carried out on the original power-law materials as well as their modified counterparts (with ε_b varying over a large range and example load-displacement curves given in Fig. 11a). The indenter angle α is also varied. The percentage error of C (between the original and modified materials) can be plotted as a function of ε_b, given in Fig. 11b for a representative indenter angle $\alpha = 70.3°$. Each line in this Figure represents modifications of one of the six original materials, and each symbol in that line denotes the percentage error of C for a tailored material characterized by a particular ε_b. The error decreases quickly with ε_b, since a higher ε_b means that the constitutive relationship of the modified material is closer to the original one (Fig. 10). In addition, the error of C is smaller when n is smaller or when E/σ_y is smaller (and the effect of n is more prominent), and this is also related to the fact that the difference between the stress-strain curves of the original and tailored materials are smaller when n and/or E/σ_y is smaller (Fig. 10 and Eq. 21).

Fig. 12 The dependency of the critical strain ε_c on the half-apex angle, α, of sharp indenters. Also shown is the linear fitting Eq. 22 (Liu et al. 2009)
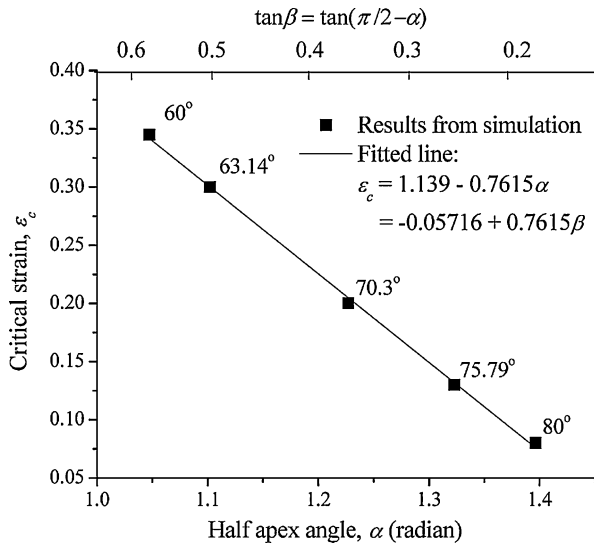
The most important finding is, regardless of the original material, the percentage error of C tends to be lower than the 1% threshold when ε_b exceeds a critical value, ε_c. For $\alpha = 70.3°$, the critical strain ε_c is identified as 0.20 – any modification of the plastic behavior beyond this point cannot be effectively reflected on the P-δ curve, and the modified material would exhibit an indistinguishable indentation response with respect to the original material as long as $\varepsilon_b > \varepsilon_c$; under this circumstance, both the original and modified materials are possible solutions of the reverse analysis of the same P-δ curve. Note that the difference between the constitutive relationships of the original material and modified material can be substantial especially when n is large and/or when the critical strain is small.

Using the sharp indentation technique, the stress-strain curve may only be probed when the strain is between 0 and ε_c (the detectable strain range or sometimes the detectable range for short). When α is fixed, ε_c is essentially material-independent, and this is verified by numerical analyses using a wide range of materials with diverse elastoplastic properties (as long as ε_y is not too large, which is satisfied for most metals and alloys). (Although we derived the critical strain by modifying the power-law material model in this section, the approach can be extended to other material models, and we have verified that the value of critical strain is not sensitive to the material model used.) In Fig. 12, the critical strain ε_c is presented as a function of the indenter angle, where the relationship is almost linear and can be fitted as

$$\varepsilon_c = 1.139 - 0.7615\alpha \tag{22}$$

within the indenter angle range in this chapter (where α is in radians in Eq. 22). It is interesting that the detectable range of sharp indenters can be small for blunt indenters, and one of the popular indenters with $\alpha = 80°$ could only prove strain

up to about 8% and thus is sensitive to the non-uniqueness issue; the use of sharper indenters could partially reduce this concern. However, sharp indenters may cause cracking, and the results may be sensitive to friction in practice. In addition, even the sharpest indenter used in this study ($\alpha = 60°$) could only detect up to 35% of strain, and this performance falls well below common expectations. We therefore conclude that it is impossible to measure the entire stress-strain curve uniquely via a sharp indentation test. (Although the plural indenter technique, especially those with sharper indenters (e.g., using $\alpha = 60°$ and $70.3°$), could alleviate the non-uniqueness problem than those with blunter indenters (e.g., using $\alpha = 80°$ and $\alpha = 70.3°$), none of them would work well outside the critical strain range.)

Besides challenging the uniqueness of indentation test, the discovery of the critical strain has several other impacts. First, during the verification of an established indentation method, often the stress-strain curve of a real engineering material needs to be fitted into power-law form and serve as a benchmark for examination (Guelorget et al. 2007); however, a different fitting range of the stress-strain curve would lead to different fitted results of the plastic parameters, and the fitting range should be consistent with the detectable range of indentation test, otherwise a large bias would occur (Ogasawara et al. 2008). Second, the critical strain could also guide numerical indentation analyses. From either the stress-strain curve measured in a lab experiment or with respect to a specific material model, a data set of the uniaxial stress and strain is needed as the input for material properties to be used in an FEM program/simulation. Sometimes there is a concern as to how many data points are needed and how refined they need to be. Here we show that regardless of the details, only the input stress-strain data within the detectable strain range is relevant, and outside this range, the data is essentially unimportant (in terms of the resulting P-δ curves).

Variation of Critical Strain: A Qualitative Explanation

A qualitative explanation of the critical strain, along with its dependency on the indenter geometry, lies in the nonuniform plastic deformation below the indenter. Since the work done by the indenter during the penetration of a sharp indenter is $W_t = C\delta^3/3$, the perturbation of C may be understood from that of W_t, which equals the total deformation energy. The material deformation energy includes two parts: the recoverable strain energy and the plastic dissipation; the later part equals $(W_t\text{-}W_e)$.

The influence of tailoring the material constitutive behavior is nonuniform in the indented solid. Within the field of equivalent plastic strain (ε_e) produced by indentation, only the regions with $\varepsilon_e > \varepsilon_b$ are more sensitive to the modification of plastic properties beyond ε_b. Figure 13 shows the contour plots of ε_e in the deformed unmodified power-law solid (with $E/\sigma_y = 2500$, and $n = 0.5$), and the contour lines of $\varepsilon_e = 0.1$ and 0.2 are given when $\alpha = 70.3°$ and $75.79°$, respectively. For fair comparison, the contours shown in Fig. 13 are taken at the instants when the indenters have done the same amount of work. The material enclosed roughly by

Fig. 13 The contour plot of the equivalent plastic strain, ε_e, in a semi-infinite solid indented by two sharp indenters. The superimposed contours are taken from independent tests at the instants when the indenters have done the same amount of work (Liu et al. 2009)

The contours of the equivalent plastic strain, ε_e, upon the penetration of two conical indenters, respectively.
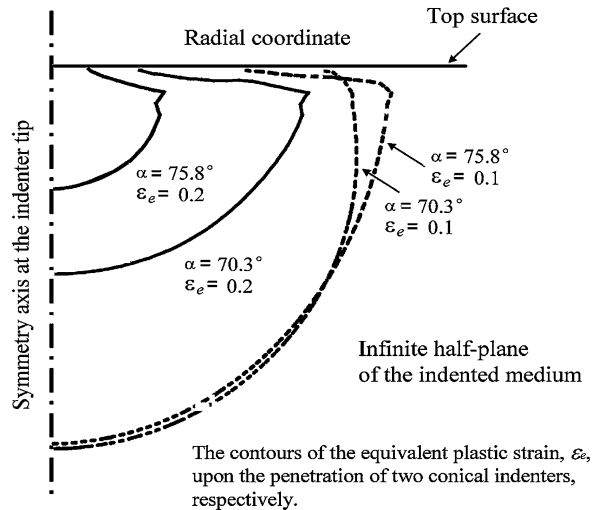
the solid contour lines (e.g., $\varepsilon_e = 0.2$) may be perturbed if the stress-strain curve is modified beyond the corresponding value, for example, $\varepsilon_b = 0.2$. Within the area where $\varepsilon_e < \varepsilon_b$, if the deformation energy is relatively small, material tailoring would not yield prominent variation of the overall indentation response.

For $\alpha = 70.3°$ for example, the deformation energy in the region enclosed by the contour of $\varepsilon_e = 0.2$ is only about 22% of the energy enclosed by the contour of $\varepsilon_e = 0.1$. Therefore, tailoring the material beyond $\varepsilon_b = 0.1$ will include a larger variation to the overall P-δ curve than tailoring above $\varepsilon_b = 0.2$. This is qualitatively consistent with the descending trend of the error of C due to tailoring Fig. 11b. When the indenter angle is varied, for $\alpha = 75.79°$, the fraction of deformation energy of the region enclosed by the contour of $\varepsilon_e = 0.2$ is only 3% of its counterpart for $\alpha = 70.3°$, and the fraction of deformation energy of the region surrounded by the contour of $\varepsilon_e = 0.1$ is about half that for $\alpha = 70.3°$. This suggests that material tailoring beyond the same strain ($\varepsilon_b = 0.1$ or 0.2) could influence C more significantly for the sharper indenter, and thus qualitatively speaking, ε_c is larger for a sharper indenter and smaller for a blunter indenter.

Conclusion

Although indentation tests have been long used to measure the elastoplastic properties of engineering materials, a systematic study on the uniqueness of indentation analysis, i.e., on the possible existence of the one-to-one correspondence between the indentation load-displacement curves, material parameters, and indenter geometries, is still lacking. Among the available indentation techniques, the dual (or plural) sharp indenter method is often considered as well established, and it is also the foundation of many other similar indentation analyses and has been widely

used in practice. In this chapter, through a comprehensive numerical study, the primary shape factors of the indentation load-displacement curves are related with the material properties and indenter angles through simple functional forms. Both explicit and numerical procedures are established to search for mystical materials with distinct elastoplastic properties yet yield indistinguishable load-displacement curves, even when the indenter angles are varied. Consequently, these mystical materials cannot be distinguished by many of the existing dual (or plural) indenter methods or spherical indenter methods (if the indentation depth is shallow). The properties and the existence of such mystical materials are discussed.

In addition, a critical strain is identified as the upper bound of the detectable range of indentation, and moderate tailoring of the constitutive behavior beyond this range cannot be effectively detected by the reverse analysis of the load-displacement curve. That is, for a given indenter geometry, beyond the critical strain, there is no unique solution of the material plastic behavior from the reverse analysis of the load-displacement curve. The critical strain is identified as a function of the sharp indenter angle, through which the analysis of sharp indentation may be qualitatively correlated to some extent – this link also enriches the indentation theory and applications.

The topics in this chapter address the important question of the uniqueness of indentation test, as well as providing useful guidelines to properly use the indentation technique to measure material elastoplastic properties.

References

J. Alkorta, J.M. Martinez-Esnaola, J.G. Sevillano, Absence of one-to-one correspondence between elastoplastic properties and sharp-indentation load–penetration data. J. Mater. Res. **20**, 432–437 (2005)

M.F. Ashby, *Materials Selection in Mechanical Design*, 2nd edn. (Elsevier, Amsterdam, 1999)

F.P. Bowden, D. Tabor, *The Friction and Lubrications of Solids* (Oxford University Press, Oxford, 1950)

Y.P. Cao, J. Lu, A new method to extract the plastic properties of metal materials from an instrumented spherical indentation loading curve. Acta Mater. **52**, 4023–4032 (2004)

T.W. Capehart, Y.T. Cheng, Determining constitutive models from conical indentation: sensitivity analysis. J. Mater. Res. **18**, 827–832 (2003)

X. Chen, N. Ogasawara, M. Zhao, N. Chiba, On the uniqueness of measuring elastoplastic properties from indentation: the indistinguishable mystical materials. J. Mech. Phys. Solids **55**, 1618–1660 (2007)

Y.T. Cheng, C.M. Cheng, Can stress–strain relationships be obtained from indentation curves using conical and pyramidal indenters? J. Mater. Res. **14**, 3493–3496 (1999)

Y.T. Cheng, C.M. Cheng, Scaling, dimensional analysis, and indentation measurements. Mater. Sci. Eng. **R44**, 91–149 (2004)

B. Guelorget, M. Francois, C. Liu, J. Lu, Extracting the plastic properties of metal materials from microindentation tests: experimental comparison of recently published methods. J. Mater. Res. **22**, 1512–1519 (2007)

L. Liu, N. Ogasawara, N. Chiba, X. Chen, Can indentation technique measure unique elastoplastic properties? J. Mater. Res. **24**, 784–800 (2009)

S.D. Mesarovic, N.A. Fleck, Spherical indentation of elastic-plastic solids. Proc. R. Soc. Lond. A **455**, 2707–2728 (1999)

N. Ogasawara, N. Chiba, X. Chen, Representative strain of indentation analysis. J. Mater. Res. **20**, 2225–2234 (2005)

N. Ogasawara, N. Chiba, X. Chen, Limit analysis-based approach to determine the material plastic properties with conical indentation. J. Mater. Res. **21**, 947–958 (2006)

N. Ogasawara, N. Chiba, M. Zhao, X. Chen, Measuring material plastic properties with optimized representative strain-based indentation technique. J. Solid Mech. Mater. Eng. **1**, 895–906 (2007a)

N. Ogasawara, N. Chiba, M. Zhao, X. Chen, Comments on "Further investigation on the definition of the representative strain in conical indentation" by Y. Cao and N. Huber [J. Mater. Res. 21, 1810 (2006)]: A systematic study on applying the representative strains to extract plastic properties through one conical indentation test. J. Mater. Res. **22**, 858–868 (2007b)

N. Ogasawara, M. Zhao, N. Chiba, X. Chen, Comments on "Extracting the plastic properties of metal materials from microindentation tests: experimental comparison of recently published methods" by B. Guelorget, et al. [J. Mater. Soc. 22, 1512 (2007)]: The correct methods of analyzing experimental data and reverse analysis of indentation tests. J. Mater. Res. **23**, 598–608 (2008)

I.N. Sneddon, The relationship between load and penetration in the axisymmetric Boussinesq problem for a punch of arbitrary profile. Int. J. Eng. Sci. **3**, 47–57 (1965)

K.K. Tho, S. Swaddiwudhipong, Z.S. Liu, K. Zeng, J. Hua, Uniqueness of reverse analysis from conical indentation tests. J. Mater. Res. **19**, 2498–2502 (2004)

M. Zhao, X. Chen, N. Ogasawara, A.C. Razvan, N. Chiba, D. Lee, Y.X. Gan, A new sharp indentation method of measuring the elastic-plastic properties of soft and compliant materials by using the substrate effect. J. Mater. Res. **21**, 3134–3151 (2006a)

M. Zhao, N. Ogasawara, N. Chiba, X. Chen, A new approach of measuring the elastic-plastic properties of bulk materials with spherical indentation. Acta Mater. **54**, 23–32 (2006b)